

A Chest-Conformable, Wireless Electro-Mechanical E-Tattoo for Measuring Multiple Cardiac Time Intervals

Sarnab Bhattacharya, Mohammad Nikbakht, Alec Alden, Philip Tan, JiETING Wang, Taha A. Alhalimi, Sangjun Kim, Pulin Wang, Hirofumi Tanaka, Animesh Tandon, Edward F. Coyle, Omer T. Inan, and Nanshu Lu*

Cardiovascular diseases are the leading cause of death globally. Noninvasive, accurate, and continuous cardiovascular monitoring can enable the preemptive detection of heart diseases and timely intervention to prevent serious cardiac complications. However, unobtrusive, ambulatory, and comprehensive cardiac monitoring is still a challenge as conventional electronics are rigid, heavy, or consume too much power for long-term measurement. This work presents a thin (200 μm), stretchable (20%), lightweight (2.5 g), wireless, and low-power (<3 mW) cardiac monitoring device that conforms to the human chest like a temporary tattoo sticker, correspondingly known as an e-tattoo. This chest e-tattoo features dual-mode electro-mechanical sensing—bio-electric cardiac signals via electrocardiography and mechanical cardiac rhythm via seismocardiography. A unique peripheral synchronization strategy between the two sensors enables the measurement of systolic time intervals like the pre-ejection period and the left ventricular ejection time with high accuracy (error = -0.44 ± 8.74 ms) while consuming very low power. The e-tattoo is validated against clinically approved gold-standard instruments on five human subjects. The good wearability and low power consumption of this e-tattoo permit 24-h continuous ambulatory monitoring.

1. Introduction

The heart is an essential organ responsible for the delivery of oxygen, nutrients, hormones, and other essential compounds to all organs of the body. As a result, chronic or acute failure of cardiac function will assuredly be followed by severe systemic complications. The Centers for Disease Control and Prevention (CDC) states that “Heart disease is the leading cause of death for men, women, and people of most ethnic groups in the United States.”^[1] In a variety of heart diseases, continuous, unobtrusive cardiac monitoring may detect disease onset or decline earlier, enabling earlier detection and intervention, and thus potentially improving outcomes.^[2,3] However, traditional cardiac monitoring instruments have been designed solely for use in laboratory or clinical settings and are unsuitable for ambulatory monitoring.

S. Bhattacharya, P. Tan
Department of Electrical and Computer Engineering
The University of Texas at Austin
Austin, TX 78712, USA

M. Nikbakht, O. T. Inan
School of Electrical and Computer Engineering
Georgia Institute of Technology
Atlanta, GA 30332, USA

A. Alden
Department of Biomedical Engineering
The University of Texas at Austin
Austin, TX 78712, USA

J. Wang, T. A. Alhalimi, H. Tanaka, E. F. Coyle
Department of Kinesiology and Health Education
The University of Texas at Austin
Austin, TX 78712, USA


S. Kim
Department of Mechanical Engineering
The University of Texas at Austin
Austin, TX 78712, USA

P. Wang
Stretch Med Inc.
Austin, TX 78750, USA

A. Tandon
Department of Pediatric Cardiology and Cleveland Clinic Children's
Center for Artificial Intelligence (C4AI)
Pediatric Institute
Cleveland Clinic Children's
Cleveland, OH 44195, USA

A. Tandon
Department of Biomedical Engineering
Lerner Research Institute
Cleveland Clinic
Cleveland, OH 44195, USA

A. Tandon
Department of Biomedical Engineering
Case School of Engineering at Case Western Reserve University
Cleveland, OH 44195, USA

 The ORCID identification number(s) for the author(s) of this article can be found under <https://doi.org/10.1002/aelm.202201284>.

© 2023 The Authors. Advanced Electronic Materials published by Wiley-VCH GmbH. This is an open access article under the terms of the Creative Commons Attribution License, which permits use, distribution and reproduction in any medium, provided the original work is properly cited.

DOI: 10.1002/aelm.202201284

Ambulatory cardiac monitoring can reveal masked problems, and provide early detection of critical physiological events, giving patients more time to seek medical help.^[4] Hence, the form factor of next-generation medical devices is evolving, with a focus on unobtrusiveness, comfort, imperceptibility, social acceptableness, complete mobility, and long-term operation without requiring recharging, all without sacrificing the accuracy and reliability of the data being collected. Rapid advances in flexible and stretchable soft bio-electronics, provide a viable solution for wearable, comfortable, and continuous health monitoring.^[5,6] This class of soft bio-electronics is able to address many of the downsides of traditional health monitoring devices with the potential to become a ubiquitous technology in the near future.

The ventricular function can be divided into four phases: isovolumic relaxation, ventricular filling, isovolumic contraction, and rapid ventricular ejection. Isovolumetric relaxation and ventricular filling constitute the ventricular diastolic phase. During the ventricular filling the mitral valve is open and blood is flowing into the ventricles. After the ventricle fills and transitions to contracting, the pressure eventually exceeds that of the atrium. This gradient closes the mitral valve, which marks the beginning of systole. The time between the closing of the mitral valve and the subsequent opening of the aortic valve is the isovolumic contraction (IVC) period. The aortic valve opens when the pressure within the ventricle exceeds the pressure in the aorta, marking the beginning of rapid ventricular ejection. After the aortic valve closes, the cycle begins again. Impairment of the heart's pumping function, known as systolic congestive heart failure, or heart failure with reduced ejection fraction, can prevent the proper flow of oxygen and nutrients to target organs. Parameters such as stroke volume (SV), cardiac output (CO), and ejection fraction (EF) provide important insight into the health and performance of the heart.^[7] However, a lack of accurate, non-invasive, and/or easy-to-use devices for measuring these parameters hinders their widespread adoption for cardiovascular health assessment.^[8] Systolic timing intervals (STI) which measure the duration of cardiac phases have been demonstrated as viable alternatives to these parameters for assessing cardiac performance.^[9] The pre-ejection period (PEP) is the time between the electrical excitation of the ventricular cardiomyocytes and the opening of the aortic valve (AO). This includes the electromechanical delay (EMD) from the electrical depolarization of the ventricles to the start of ventricular contraction as well as the IVC time. PEP provides insight into myocardial contractility as an increase in contractility results in a sharper increase in left ventricular (LV) pressure thereby shortening the PEP.^[10,11] The left ventricular ejection time (LVET) is the

time from AO to the closure of the aortic valve (AC) and represents the total time blood flows from the ventricle into the aorta. The sum of these two periods (electromechanical systole or QS₂) is the total time the heart spends in ventricular systole. The PEP and LVET offer a convenient non-invasive method to assess LV performance.^[9] People suffering from heart failure exhibit a lengthening of PEP and shortening of LVET mostly due to a diminished rate of isovolumetric pressure rise, and an inability to maintain a high LV pressure during the ejection period associated with decreased cardiac contractility, respectively.^[12] As a result, it has been proposed that the ratio between PEP and LVET is a good indicator of LV dysfunction.^[13]

Although common, solely using an electrocardiogram (ECG) to track cardiac health is limited as it can only sense the electrical activity of the heart and is unable to provide any information about the mechanical activity of the heart such as contraction and valve activity. Several non-invasive methods for capturing these mechanical cardiac events have been introduced. Impedance cardiography (ICG) devices measure the impedance change caused by blood being pumped by the heart, and the features from the corresponding impedance waveform can be related to different cardiac events, such as AO. In healthy subjects with low body mass index (BMI), this technique can provide accurate measures of STIs; however, in broader populations with cardiovascular diseases and in patients with higher BMI, ICG has been shown to have high error compared to reference standard invasive measures.^[14,15] Additionally, ICG requires electrodes spaced across the whole thorax, requiring trained personnel for positioning and making unobstructed monitoring very difficult. Phonocardiograms (PCG) capture the acoustic signals generated by the heart valves. However, cardiac acoustic signals are only generated by the closure of the valves and thus cannot provide any indication of the opening of the aortic valve as needed for both PEP and LVET.^[16] More recently ballistocardiogram (BCG) and seismocardiogram (SCG) measurements have become popular for mechanical heart function assessments.^[17] The BCG signal is caused by the motion of the whole body generated by the ejection of blood by the heart and the movement of blood through the vasculature but requires special scales or beds to capture. The SCG signal is a more localized measurement of the chest vibrations associated with cardiac contraction and blood movement, usually measured at or near the sternum. While similar to PCG, SCG senses in a much lower frequency range (up to 40 Hz) compared to PCG (up to 750 Hz).

Here, we design, fabricate, and assemble a thin, macro-conformal, stretchable, and lightweight sensing platform that can be laminated onto the human chest like a temporary tattoo and hence termed an electronic- or e-tattoo. The e-tattoo uses dual-mode electro-mechanical sensing by utilizing ECG and SCG sensors. The ECG sensor interfaces with the human body via bio-compatible graphite film electrodes and the SCG is measured using a high-resolution, low-noise accelerometer that can detect subtle vibrations caused by the heart. Wireless connectivity incorporating Bluetooth low energy (BLE) is utilized to stream the data in real-time to a host device. External synchronization between the ECG and SCG ensures high cross-modality timing accuracy. This also allows us to reduce

N. Lu
Department of Aerospace Engineering and Engineering Mechanics
Department of Electrical and Computer Engineering
Department of Mechanical Engineering
Department of Biomedical Engineering
Texas Materials Institute
The University of Texas at Austin
Austin, TX 78712, USA
E-mail: nanshulu@utexas.edu

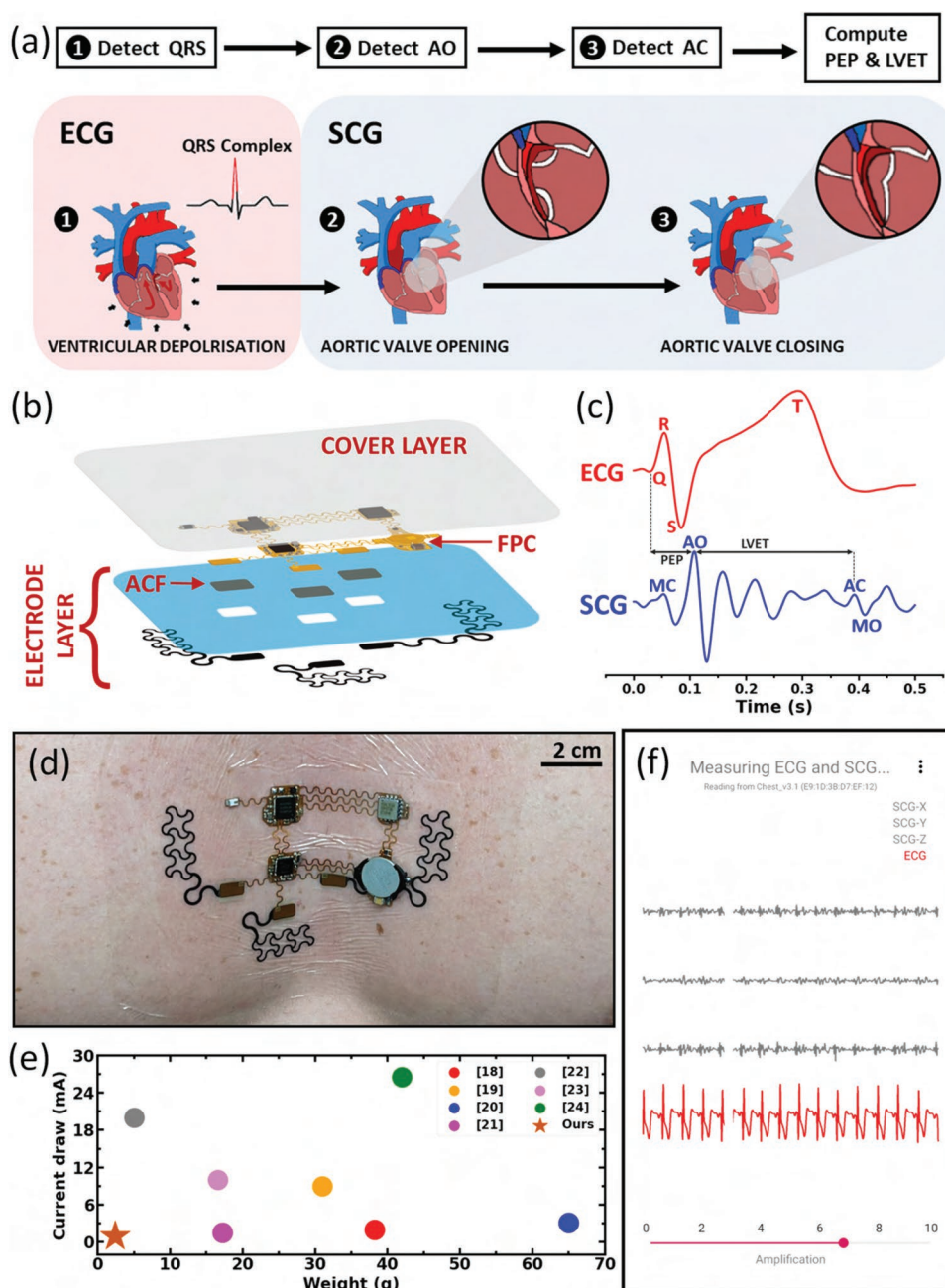


Figure 1. Introduction to systolic time intervals (STIs), e-tattoo overview, and comparison to related work. a) Different heart events captured via different modalities and used to calculate pre-ejection period (PEP) and left ventricular ejection time (LVET). b) Exploded schematic illustration of the wireless, dual-mode chest e-tattoo. Three layers from top to bottom are cover layer, flexible printed circuit (FPC), and electrode layer. c) Synchronized real electrocardiogram (ECG) and seismocardiogram (SCG) signals with important features annotated including QRS complex and T-peak on ECG, aortic valve opening (AO), aortic valve closing (AC), mitral valve closing (MC), and mitral valve opening (MO) on SCG. d) Photograph of the e-tattoo conforming to the curvature of the chest. e) Comparison of e-tattoo device weight and system current draw with similar wearable cardiac devices reported in the literature. f) Custom-designed mobile application interface for recording, visualizing, and annotating data.

power consumption to the absolute lowest level when compared to previously reported work. The e-tattoo signal quality was validated against gold-standard clinical devices, and a five person human-subject trial was conducted to characterize the accuracy and generalizability of this platform. Furthermore, a long-term wearability test with a single subject was conducted to showcase the feasibility of ambulatory cardiac monitoring.

2. Results and Discussion

Our goal is to accurately compute PEP and LVET from simultaneous ECG and SCG measurements. For that, we have to be able to detect the QRS complex on the ECG and the AO and AC events on the SCG (Figure 1a). Our device stack-up is shown in an exploded view in Figure 1b. It comprises a flexible printed

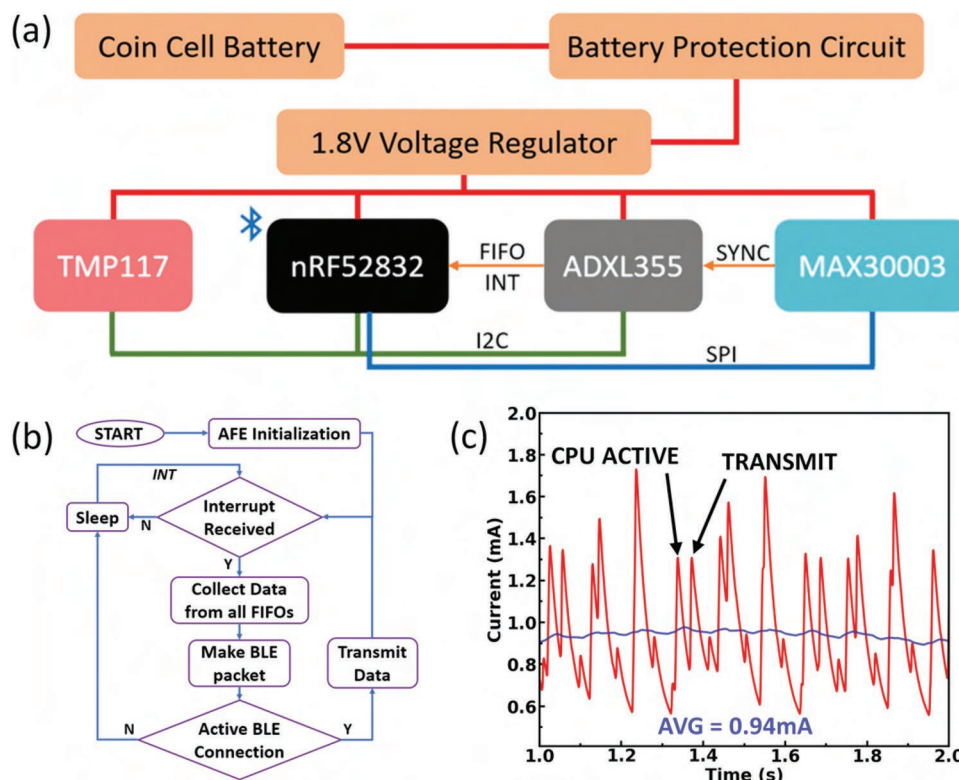


Figure 2. Circuit design, firmware flow, and power draw of the e-tattoo. a) A block diagram of the major hardware components of the e-tattoo. b) A diagram of the firmware flow for data collection and transmission. c) Active power draw of the e-tattoo during operation. The average current draw is shown in blue.

circuit (FPC) layer over an electrode layer. The electrodes are made from graphite polyurethane film and laminated onto Tegaderm. Electrical contact is made with the electrodes through holes cut out from the Tegaderm layer and anisotropic conductive film acts as an adhesive between electrodes and electronics. Electrode contact resistance is important for good ECG signal quality. Our test with stretching the serpentine graphite film electrode design showed negligible resistance change up to 40% strain (Figure S1c, Supporting Information). The FPC layer is covered with another layer of Tegaderm with a portion removed to expose the battery. It should be noted that the electronics are completely isolated from contact with the human body and the only components in direct skin contact are the graphite film electrodes and the medical dressing. Figure 1c shows the synchronized ECG and SCG waveforms ensembled over five heartbeats to reduce noise with the relevant cardiac features (e.g., QRS complex, AO, AC) marked. Our flexible, lightweight, and stretchable design allows the e-tattoo to conform to the macro contours of the human body for easy lamination on the human chest as shown in Figure 1d. This form factor coupled with innovative firmware for sensor interfacing and transmission of data allows us to achieve one of the lowest total device weights (2.5 g including battery) and current draws (940 μ A) among wearable cardiac sensors developed in prior work as illustrated via Ashby plot in Figure 1e.^[18–24] The ECG, SCG, and other acquired data (e.g., temperature, packet count) is transmitted in real-time over BLE to a host device such as a mobile phone. We have developed a custom mobile application

to connect to our e-tattoo and receive and store the streamed data for later use. The application also offers an easy-to-use user interface for visualizing the data in real-time for verifying the signal quality and marking important events (Figure 1f). Markers that are placed using this interface are parsed as labels at specific timestamps in post-processing, allowing the user to annotate the data properly. Figure S2, Supporting Information, illustrates using the mobile application to record data and record user-defined markers.

The electronic subsystem illustrated in Figure 2a consists of a central processing unit (CPU) with BLE capabilities. We have chosen the nRF52832 from Nordic semiconductor for its ultra-low power consumption and sufficient processing power to perform required firmware tasks. The sensors are connected via different buses to the CPU. The ECG front end (MAX30003, Maxim Integrated) is a single lead ECG sensor with a right leg drive connected to the CPU over the serial peripheral interface (SPI). The ECG sensor contains analog high-pass and low-pass filters. The high pass filter (cutoff frequency = 0.5 Hz) filters out any DC drift in the ECG signal. The low pass filter (cutoff frequency = 40 Hz) performs anti-aliasing and high-frequency noise reduction. The SCG sensor (ADXL355, analog devices), is a high-resolution, low-noise, micro-electromechanical system (MEMS)-based accelerometer from analog devices connected to the CPU over the inter-integrated circuit (I2C) interface. Both these integrated circuits are completely self-sufficient (i.e., integrated analog front end, analog-to-digital converter, and digital readout), thus requiring minimal external components which

reduces external noise contamination and power consumption. A digital temperature sensor (TMP117, Texas Instruments) sharing the I2C bus is located on the bottom side of the FPC allowing for more direct measurement of the skin. Although data from the temperature sensor is not used for extracting STIs, it is still a useful biometric for detecting fever.^[25] The temperature sensor accuracy was compared to a standard thermistor (TMD-56, Amprobe) over a wide range of temperatures and was found to have very little error ($0.14 \pm 0.07^\circ\text{C}$, Figure S1d, Supporting Information). To achieve high accuracy in detecting STIs the sampling interval must be free of variability. Furthermore, the synchronization between the ECG and SCG sensors also has to be very accurate, that is, clock jitter and clock drift have to be kept at a minimum. This is especially true when trying to extract the PEP as it requires signals from separate sensors (i.e., ECG and SCG) and is much more sensitive to measurement error due to its relatively short absolute length (≈ 100 ms). Our data acquisition scheme achieves sub-ms-level synchronization while keeping power consumption to a minimum. To reduce clock jitter, we use an external 32.768 KHz crystal (KX201, Diodes Incorporated) with superb frequency stability (25 PPM) over a wide range of operating conditions to generate the sampling clock for the ECG sensor. To prevent clock drift between the ECG and SCG, we use a hardware synchronization method where the ECG sensor generates a *sync* pulse on every sample. The SCG sensor uses this pulse as an external sampling trigger. This ensures the samples on both sensors occur at the same time with a small, fixed, and deterministic delay. Both the sensors have internal queues (FIFOs) for storing data and this synchronization method makes it possible for the sensors to autonomously sample and store data locally without intervention from the CPU which can remain in a low-power sleep state. Once the FIFOs are full an interrupt signal is sent to the CPU which wakes up to collect the stored data from both sensors, compress it, and transmit it to a host device. This firmware flow is illustrated in Figure 2b. The ECG and SCG sensor is sampled at 125 Hz and the FIFO size is kept at 20 samples, which translates to a CPU wake frequency of 6.25 Hz. Since the CPU, the most power-hungry component, is kept in sleep mode most of the time, the average current draw of the e-tattoo while actively transmitting data is less than 1 mA with occasional spikes up to 2 mA when the CPU becomes active and/or data is transmitted over BLE as shown in the current draw graph in Figure 2c. Power is supplied to the e-tattoo from a small form factor coin cell battery (CR1220) which is capable of providing power for up to 40 h of operation. Analog filters smooth out any potential current spikes from damaging the battery and a low drop-out (LDO) voltage regulator (NCP170, Onsemi) ensures proper voltage is supplied to the circuit components.

There have been multiple previous works that have delved into using dual-mode ECG and SCG sensing for cardiac time intervals measurements.^[26–29] Our goal was to make a sensing platform that was unobtrusive and minimally intrusive for enhanced user comfort. To be comfortable to wear, our e-tattoo needs to conform to the macro contours of the body specifically the sternal region of the chest. It also needs to stretch along with the skin when the user changes their posture or is in motion. We utilize serpentine interconnects^[30,31] between different groups of electronics to enable our e-tattoo to stretch reliably

up to 20% strain (applied uni-axially) without any damage or drop in signal quality (Figure 3a–c). It should be noted that for obtaining the post-stretch data shown in Figure 3c, the e-tattoo was relaxed and then reapplied on the human subject. Data collected from human subjects also indicate the maximum tensile strain of the central chest region is less than 20% (Figure S3, Supporting Information). The e-tattoo also functions well under compressive strain and no delamination of electrodes was observed (Video S4, Supporting Information). Figure 3d,e compares the e-tattoo to a rigid device performing the same function, where the e-tattoo shows conformable contact while the rigid device shows delamination on the sternal crest. Figure 3f demonstrates the easy re-usability of our e-tattoo. The covering tape and electrode layer along with the anisotropic conductive film (ACF) can be peeled away and a new electrode layer can be attached. The electronics can be re-used multiple times with new electrode layers. This reduces the operational cost of the device as the electrode layer and covering tape is much cheaper than the electronics. Multiple peeling cycles do not damage the electronics significantly and there is no perceptible damage observed after reusing ten times (Figure 3g,h). The ECG signal from a new e-tattoo and ten times reused one also shows no major differences in signal quality (Figure 3i).

As a validation of the acquired e-tattoo signals, data from the ECG and SCG sensors were compared against data from standard clinical medical instruments. First, the ECG signal acquired from both graphite film dry electrodes and commercial Ag/AgCl-based gel electrodes (Figure 4a,b) were compared. The centroid location of both types of electrodes was kept the same to minimize the effects of electrode position. Figure 4c shows the ECG signals from both electrodes have a similar signal-to-noise ratio (SNR) and a very well-defined QRS complex. The elevated T-wave is a result of the short inter-electrode distance and not an issue caused by the dry electrodes themselves, evident both by the waveform acquired from the gel electrodes placed in the same location and in the literature.^[18,32–34] As the focus of this device is the accurate extraction of STIs, only the QRS complex needs to be accurate. We opted to use dry electrodes as we envisioned our e-tattoo being applied on users for an extended duration of time. Previous work has already shown the disadvantage of using gel electrodes for long durations.^[35,36] It should also be noted that as the gel dries during extended use the electrode contact impedance rises sharply which makes the signal susceptible to external noise.^[37] Figure 4d shows the SCG signal collected with the e-tattoo compared against an M-mode echocardiogram. The e-tattoo and echocardiogram were synchronized using the ECG signal captured on both systems. From this comparison, the AO clearly corresponds to the first major peak of the first heart sound, and the AC is near the beginning of the first major minima of the second heart sound. This result agrees with previous literature.^[38,39] In addition to measuring the valvular activity of the heart, the accelerometer can be used to determine the rough orientation of the user by analyzing the low-frequency (< 0.5 Hz) components. The general orientations while lying supine, standing upright, and lying on the side are detected as shown in Figure 4e. Segments of substantial motion, occurring mostly during posture change, can also be detected and are marked with a pink band in Figure 4e. To test the performance of the SCG sensor

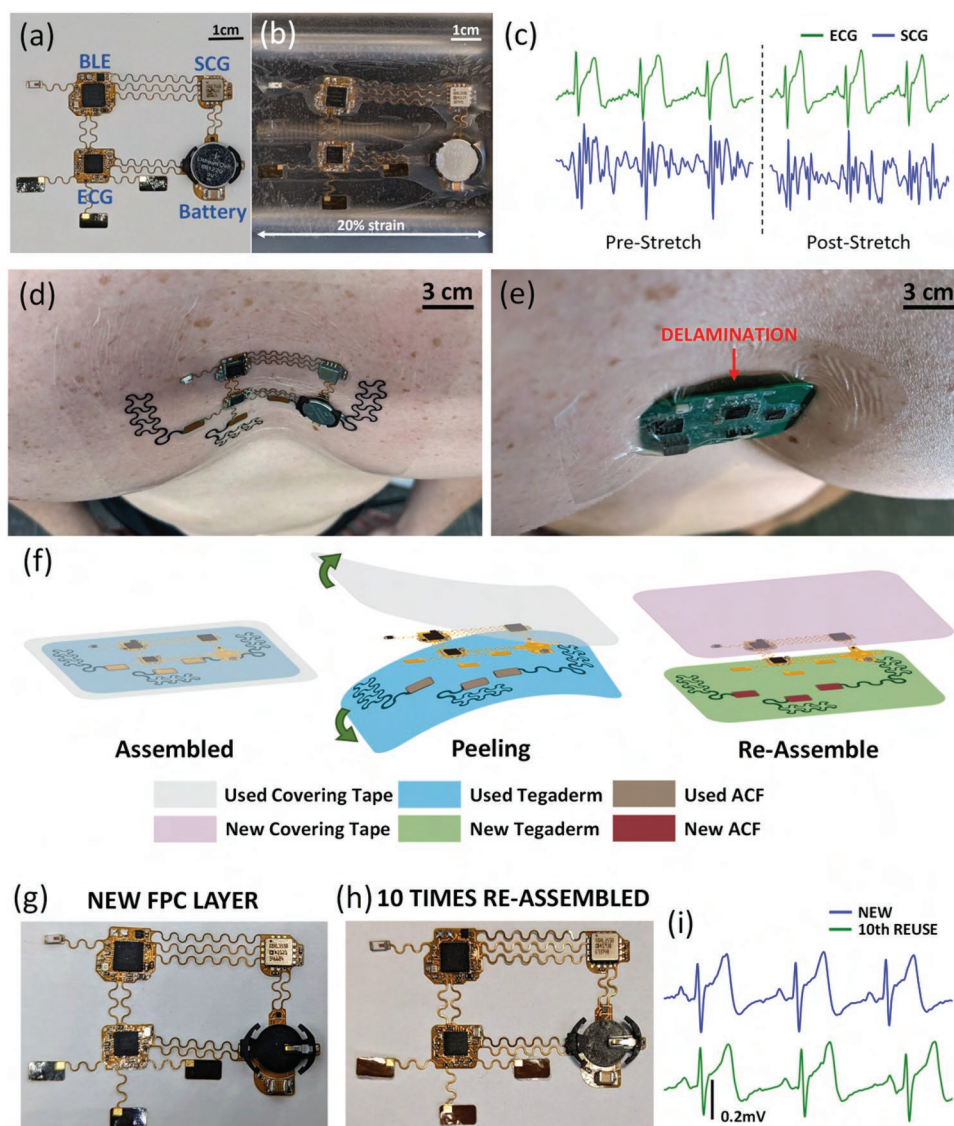


Figure 3. Mechanical performance of the chest e-tattoo. a) Optical image of the assembled flexible printed circuit (FPC) of the e-tattoo. b) Serpentine interconnects enable stretching up to 20% without damage. c) Signal quality before and after off-chest stretching and reapplication on the chest shows no significant degradation. Photographs comparing d) the e-tattoo and e) its rigid counterpart mounted on the same human chest where the e-tattoo shows conformable contact while the rigid device shows a gap from the sternum. f) Schematic illustration of the re-usability of the e-tattoo FPC by peeling off the used electrode layer and cover layer and reassembling with new ones. Photos illustrating g) a new e-tattoo FPC layer and h) the FPC layer after undergoing ten cycles of reassembly and reuse. i) electrocardiogram signals measured by new FPC (blue) and ten-time-reused FPC (green) do not show any perceptible differences.

introduced here, we re-implemented a synthetic voltage and vibration-generating phantom for replicating human-like ECG and SCG signals from our prior work.^[40] Using this system we evaluated the quality of our collected SCG signals against the known signal input to the phantom (Figure 4f).^[40] Both synthetic SCG signals (Figure 4g) and real human SCG signals (Figure 4h) were fed into the generator and were accurately reproduced by the e-tattoo.^[40,41]

A block diagram of the pre-processing pipeline designed for extracting SCG features is shown in Figure S4, Supporting Information. First, we extract the R-peaks from the ECG signals after filtering the ECG using a band-pass filter with 0.5–40 Hz cutoff frequencies.^[42] We then filter the SCG signals with a

band-pass filter (1–40 Hz) and segment the SCG signals beat-by-beat using the extracted R-peaks.^[41,43,44] Next, we apply a signal quality indexing (SQI) method for SCG beats to exclude the beats corrupted by noise above a certain threshold.^[45] For SQI we set the exponential factor (λ) to 25 and the threshold to 0.5 as suggested in prior work.^[41,46] Finally, we extract the AO and AC time locations using an SCG peak tracking algorithm introduced in prior work.^[46] We finally calculate the heart rate (HR), PEP, and LVET using the extracted R-peak, AO, and AC timings.

To test our cardiac e-tattoo system, we conducted a set of experiments on six human subjects, split into two groups of five and one for two sets of experiments. All experiments were done

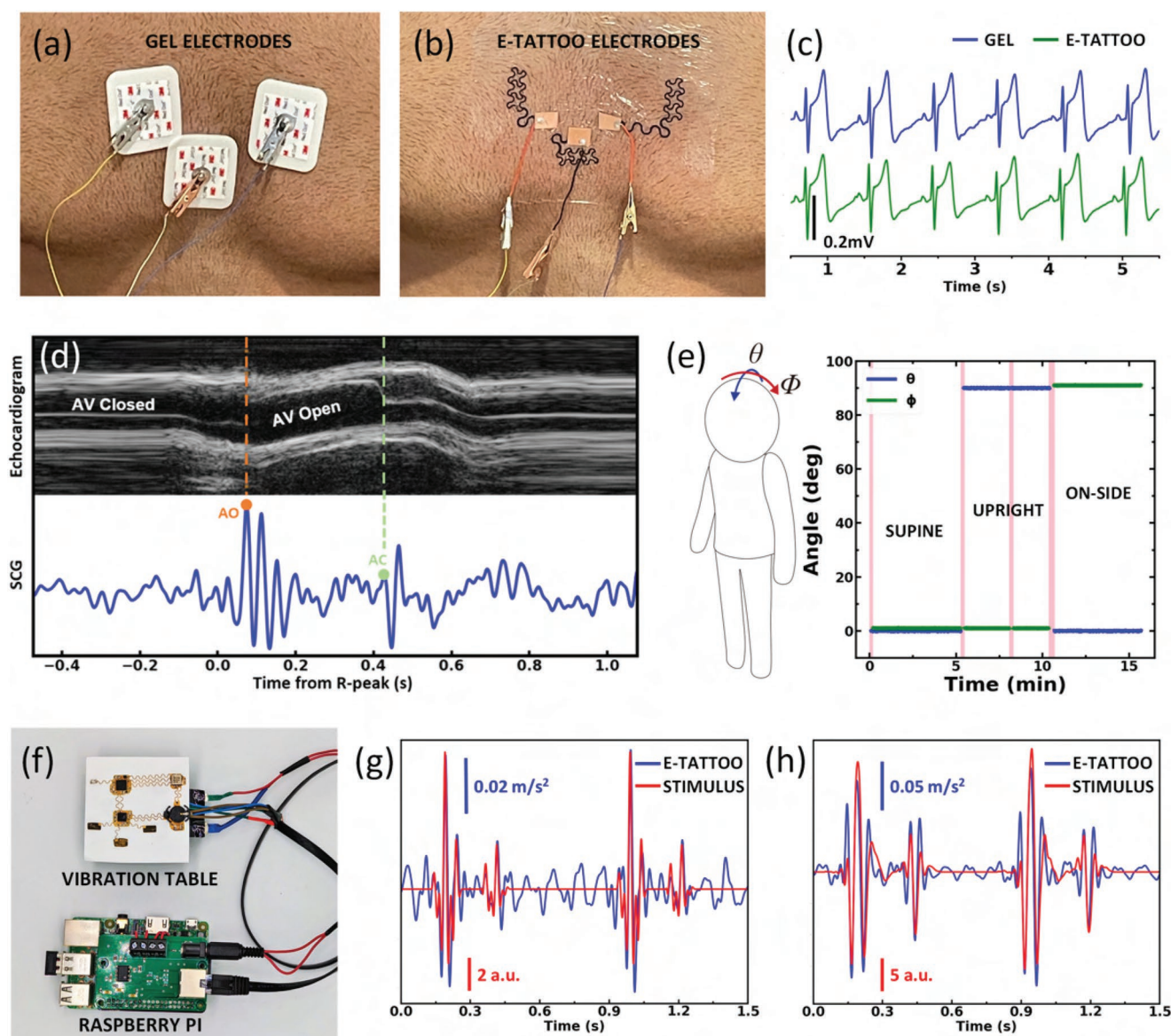


Figure 4. Individual validation of electrocardiogram (ECG) and seismocardiogram (SCG) sensors. a) Gel electrodes and b) dry e-tattoo electrodes applied on a human chest. c) ECG signals from both electrodes have similar SNR and well-defined QRS complex. d) SCG signal compared with M-mode echocardiogram. Aortic valve opening (AO) and aortic valve closing (AC) events in the echocardiogram correlate to defined features on the SCG signal. e) Orientation of the human subject can be identified from the SCG signals. f) Photograph of the platform used to test the performance and signal quality of the SCG sensor ex vivo. The SCG sensor is able to detect the AO and AC peak from simulated chest vibrations generated from g) synthetic and h) real human SCG signals, both implemented by the platform.

under an Institutional Review Board (IRB) approved protocol at the University of Texas at Austin with IRB ID STUDY00002313. Informed consent was obtained from all subjects involved in the study. The first set of experiments, conducted on five participants, consisted of holding static poses and performing cycling under incremental load with breaks (Figure 5a). Subjects simultaneously wore our e-tattoo along with a non-invasive cardiac output monitor (NICOM) (Starling Fluid Management Monitoring System, Baxter). The NICOM was used to measure multiple hemodynamic parameters including HR and LVET which was compared against data from the e-tattoo. The Bland Altman plot in Figure 5b comparing HR from the e-tattoo and

the NICOM during the static poses experiment shows a strong agreement for all participants with a difference of 0.07 ± 1.21 beats per minute (bpm). Figure 5c,d shows the change in average PEP and LVET respectively, measured in milliseconds (ms), for different participants as they transitioned from lying supine to sitting upright and then to standing. The increase in PEP and the decrease in LVET is well documented in prior literature^[26,47] and is attributed to changes in preload, contractility, and afterload. Statistically significant differences in both PEP ($p < 0.05$, paired t -test) and LVET ($p < 0.005$, paired t -test) were observed when the subjects transitioned from supine to both upright and standing. This demonstrates the capability of

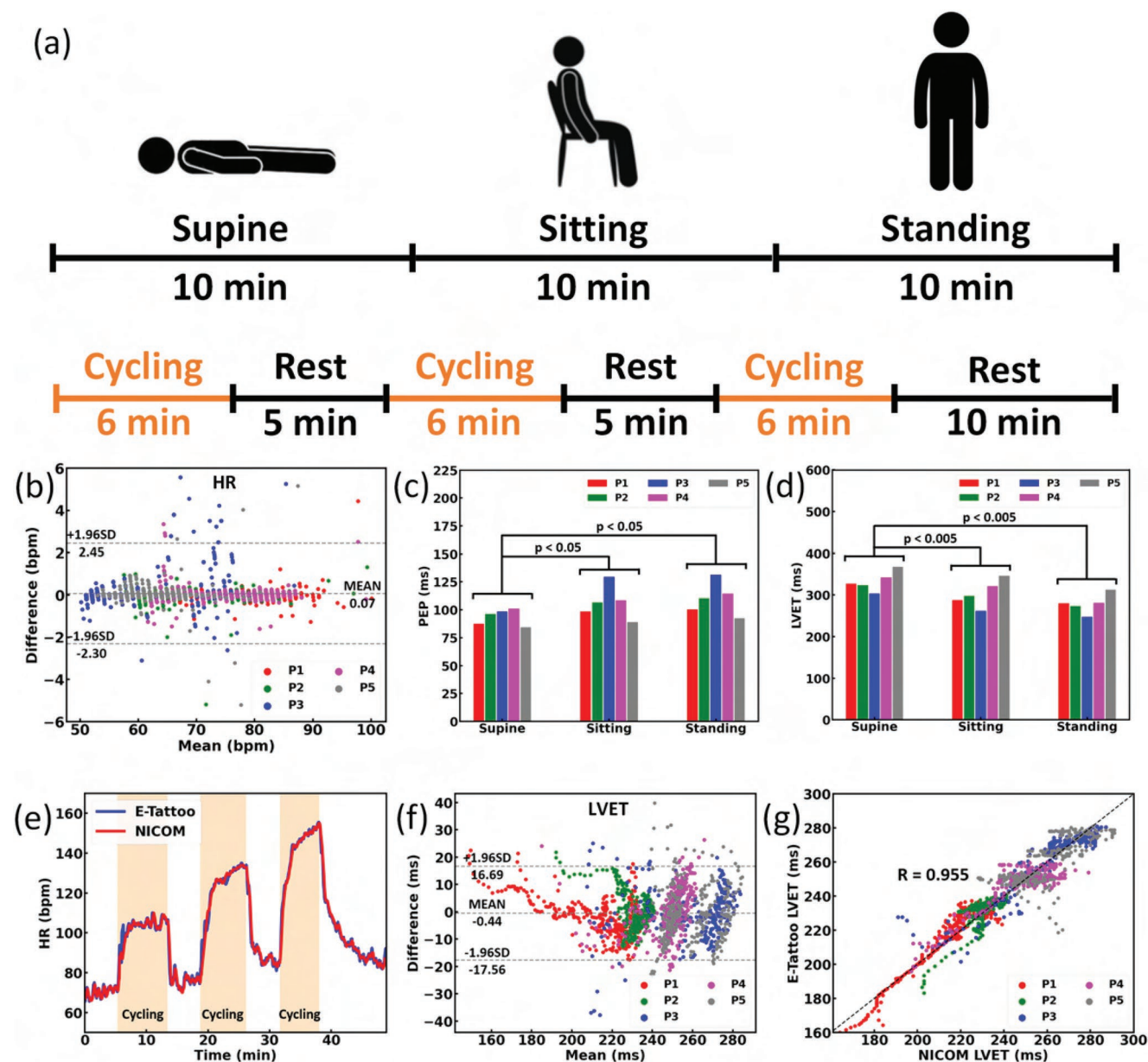


Figure 5. Human subject testing protocol and results. a) Illustration of Institutional Review Board-approved human subject testing protocol for inducing small and large changes in heart rate (HR) and systolic time intervals. b) Bland–Altman plot comparing HR from e-tattoo to HR from the non-invasive cardiac output monitor (NICOM) during static posture testing. c) Bar plot illustrating pre-ejection period (PEP) change for different participants in different postures. d) Bar plot illustrating left ventricular ejection time (LVET) change for different participants in different postures. e) Time series HR data from e-tattoo and NICOM during incremental cycling exercise. f) Bland–Altman plot comparing LVET from e-tattoo to LVET from NICOM during the rest intervals after cycling exercise. g) Correlation between LVET simultaneously measured by e-tattoo versus NICOM during the same intervals.

our e-tattoo to measure small changes in STIs caused by posture changes. Figure 5e shows the HR from the e-tattoo and from the NICOM during the cycling exercise experiment. HR from the e-tattoo is highly correlated to HR from the NICOM with a difference of 0.02 ± 1.24 bpm. Thanks to the high conformability of the e-tattoo, the ECG signal remains pristine during cycling; however, the SCG signal is corrupted by excess motion during cycling and thus no useful cardiac event data can be extracted. As a result, we choose to compute STIs during

the rest segments after every cycling segment. The rest segments were significantly less corrupted by motion artifacts while containing important hemodynamic recovery information. Figure 5f shows the Bland–Altman plot comparing the LVET from the e-tattoo and NICOM for each participant for the entire cycling experiment. Each participant exhibited different cardiovascular responses to exercise as is evident from the variation from the resting LVET. The mean difference of LVET between the two devices is -0.44 ± 8.74 ms. Our e-tattoo's

Table 1. Accuracy comparison of measuring left ventricular ejection time (LVET) reported in the literature to the e-tattoo.

Reference	Ground truth	No. of subjects	Wearable	LVET error	
				Mean [ms]	SD [ms]
This work	NICOM (ICG)	5	Yes	0	9
[49]	Aortic doppler	13	No	−14	9
[50]	Tissue doppler	85	No	−4	14
[51]	ICON-core (ICG)	10	Yes	22	24
[52]	Echo doppler	46	No	0	40
[53]	Phonocardiogram	10	No	5	86

SD; standard deviation; ms, milliseconds; ICG, impedance cardiogram.

accuracy exceeds that of other relevant works in this field as seen in Table 1. Figure 5g shows the correlation plot between the LVET measurements from the e-tattoo and the NICOM with a Pearson correlation coefficient of 0.955. This shows a very linear, one-to-one relationship between the measurements from the two devices. This demonstrates that the e-tattoo can be a viable alternative to such bulky and expensive clinical

monitors for measuring STIs. For the last experiment, we performed a long-term ambulatory study on one participant for more than 24 h. Due to the non-portability of the NICOM and the lack of any wearable LVET or PEP measuring devices, we could not compare the e-tattoo's long-term LVET and PEP data against a reference device. The goal of the study was to validate if e-tattoos can be unobtrusive, and minimally obstructive wearable devices that can be worn in day-to-day lives and in most social settings. Keeping this in mind we opted to use a Samsung Galaxy Watch 3 for long-term HR comparison (Figure 6a). As mentioned previously, the SCG signal is unusable during significant motion. However, there are many segments of time during our daily lives where motion is minimized, such as working at a computer, waiting at the traffic light while driving, taking a pause while walking, and during sleep. The long-term data was manually inspected to find these *restful* segments and it can be observed in Figure 6b–d that the ECG and SCG data is mostly devoid of any motion artifacts. These segments are ideal for extracting STIs and contextualizing them to the activity being performed would provide a more holistic understanding of the cardiovascular health of the user. Sleep monitoring is also a very important aspect as motion artifacts are kept to a

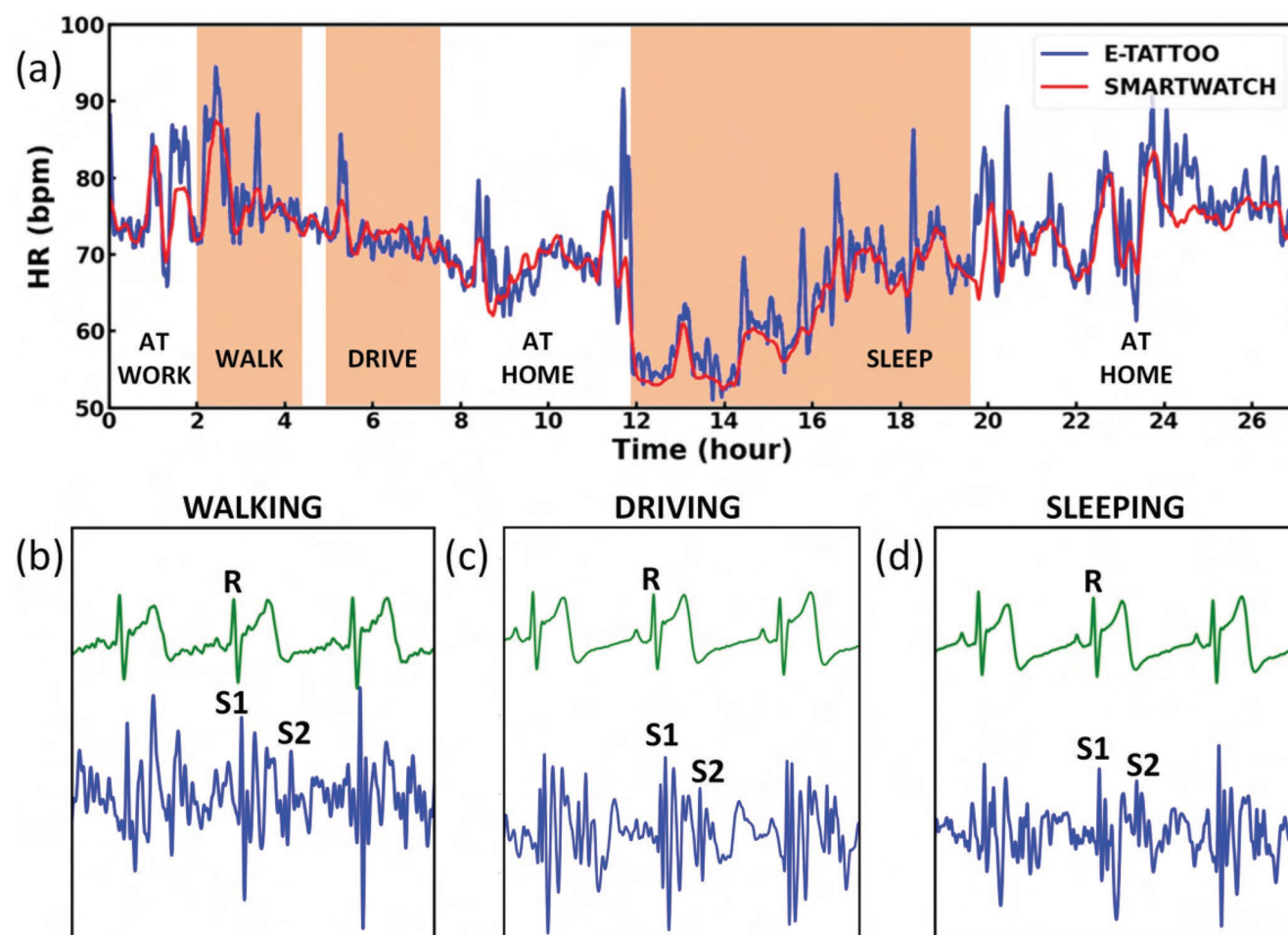


Figure 6. Long-term continuous and ambulatory sensing using e-tattoo. a) Time series heart rate (HR) data from e-tattoo and Samsung Galaxy smartwatch during a 24-h period. b–d) The electrocardiogram signal (green) and the seismocardiogram signal (blue) from the rest intervals after different activities performed in the 24-h period.

minimum and sleep hemodynamics offer unique insight into cardiovascular regulation mechanisms in pathological conditions associated with sleep disorders such as sleep apnea and insomnia.^[48]

3. Conclusion

In summary, STIs are important indicators of many different cardiovascular diseases but are only measurable through invasive means in the current medical practice. We have designed, built, and tested a thin and stretchable chest e-tattoo capable of wireless and mobile sensing of ECG and SCG. By employing an innovative peripheral synchronization technique for ECG and SCG sensors, we accomplished remarkably low ECG–SCG jitter and high energy efficiency. The lightweight and chest conformability of the e-tattoo not only afford exceptional wearability but also enable high-fidelity SCG measurement. Through both electrical and mechanical innovations, we ultimately achieved the accurate extraction of the STIs. The e-tattoos were validated against standard clinical apparatus and instruments and demonstrated their efficacy in capturing equivalent signals and data. The e-tattoo has been successfully applied on five healthy subjects and has shown a high correlation in detecting HR and LVET with errors of 0.02 ± 1.24 bpm and -0.44 ± 8.74 ms, respectively during exercise recovery. 24-h continuous and mobile cardiac sensing using the chest e-tattoo has been demonstrated and a good correlation with consumer smartwatch has been found. Our work manifests that chest e-tattoos have the potential to eventually become a medical-grade, long-term, ambulatory cardiovascular monitoring tool.

4. Experimental Section

Device Fabrication and Assembly: The electronics consisted of a double-layer FPC with polyimide (PI) as the substrate and copper traces on top and bottom. It was encapsulated with additional PI layers on both sides to prevent unintentional electrical contact. The exposed copper for connecting to the integrated circuits (IC) and other circuit components underwent an electroless nickel immersion gold (ENIG) surface plating process. The total thickness of the FPC was around 100 μm , and a more detailed FPC stack-up is shown in Figure S5, Supporting Information. The circuit components were soldered onto the FPC with lead (Pb) free soldering paste to make it safer for use on human subjects. The FPC was patterned in an island-serpentine design comprising islands of densely packed electronics connected by stretchable serpentine interconnects. The electrode for the ECG was made with graphite film (graphite polyurethane film, Mineral Seal Corporation) which had been laser cut into serpentine-like patterns to make it stretchable. Using the “cut-and-paste” subtractive manufacturing process introduced by the authors,^[54] the graphite film was transferred onto commercial medical dressing (Tegaderm, 3M) and is illustrated in Figure S6, Supporting Information. Without active circuit components, the total thickness of the FPC and electrode layer was only 200 μm .

Small holes were cut on the medical dressing to expose a part of the electrodes where a piece of ACF was attached. The ACF material was epoxy/acrylate-blend adhesive system filled with 43-micron silver-coated glass beads (Anisotropic Conductive Film 7303, 3M). After the electronics were mounted over the ACF, pressure was applied to activate the ACF and form an electrical connection between the electrodes and the ECG front end.

Human Subject Recruitment Method: Recruitment flyers were posted on university notice boards to recruit participants for this study. The inclusion criteria were healthy individuals, without physical disabilities, between the ages of 18 to 40 years. The exclusion criterion was anyone with a known history of cardiovascular disease. Five healthy males between the ages of 20 to 28 were chosen for the first human subject trial and a male aged 27 was chosen for the long-term study. The participants were chosen based on varying BMI and musculature as it was believed these would be the two main factors to influence the performance of the e-tattoo.

Supporting Information

Supporting Information is available from the Wiley Online Library or from the author.

Acknowledgements

This research was sponsored by the US Office of Naval Research under Grant No. N00014-20-1-2112, and the National Science Foundation Grants STTR-1938254 and ASCENT-2133106. O.T.I. is supported by the Linda J. and Mark C. Smith Chair funds at Georgia Tech. A.T. would like to acknowledge support from the Thrasher Foundation Early Career Research Award, Brett Boyer Foundation, Children’s Health Innovation Grant, Cleveland Clinic Caregiver Catalyst Grant, UT Southwestern Cary Council/DocStars/Southwestern Medical Foundation, and UT Southwestern Center for Translational Medicine Swim with the Sharks Grant.

Conflict of Interest

O.T.I. is a co-founder and board member of Cardiosense, Inc. A.T. is a consultant for Synergen Technology Labs, LLC, and Siemens Healthineers. P.W. is the managing director of Stretch Med Inc.

Author Contributions

Idea conception and design: S. B., M.N., P.T., O.T.I., N. L., device design and fabrication: S.B., A.A., P.T., device testing and validation: S. B., A.A., T.A. A., S.K., P.W., H.T., N.L., data analysis and interpretation of results: S.B., M.N., P.T., A.T., O.T.I., N.L., draft manuscript preparation: S.B., M.N., P.T., S.K., A.T., O.T.I., N.L., securing funding: N.L., E.F.C., P.W. All authors reviewed the results and approved the final version of the manuscript.

Data Availability Statement

Research data are not shared.

Keywords

cardiovascular monitoring, electrocardiogram, seismocardiogram, stretchable electronics, wearable electronics

Received: November 30, 2022

Revised: February 1, 2023

Published online:

- [1] Heart disease facts, <https://www.cdc.gov/heartdisease/facts.htm> (accessed: October 2022).
- [2] Y. Khan, A. E. Ostfeld, C. M. Lochner, A. Pierre, A. C. Arias, *Adv. Mater.* **2016**, 28, 4373.
- [3] I. You, B. Kim, J. Park, K. Koh, S. Shin, S. Jung, U. Jeong, *Adv. Mater.* **2016**, 28, 6359.
- [4] B. M. Kuehn, *Circulation* **2016**, 134, 1189.
- [5] H. Jeong, L. Wang, T. Ha, R. Mitbender, X. Yang, Z. Dai, S. Qiao, L. Shen, N. Sun, N. Lu, *Adv. Mater. Technol.* **2019**, 4, 1900117.
- [6] Y. J. Hong, H. Jeong, K. W. Cho, N. Lu, D.-H. Kim, *Adv. Funct. Mater.* **2019**, 29, 1808247.
- [7] Z. S. Bruss, A. Raja, *Physiology, Stroke Volume, StatPearls*, StatPearls Publishing, Treasure Island, FL **2022**.
- [8] M. Sanders, S. Servaas, C. Slaght, *J. Clin. Monit. Comput.* **2020**, 34, 433.
- [9] S. Hassan, P. Turner, *Postgrad. Med. J.* **1983**, 59, 423.
- [10] S. S. Ahmed, G. E. Levinson, C. J. Schwartz, P. O. Ettinger, *Circulation* **1972**, 46, 559.
- [11] R. P. Lewis, S. Rittogers, W. Froester, H. Boudoulas, *Circulation* **1977**, 56, 146.
- [12] A. M. Weissler, W. S. Harris, C. D. Schoenfeld, *Circulation* **1968**, 37, 149.
- [13] H. Boudoulas, *Eur. Heart J.* **1990**, 11, 93.
- [14] A. Quain, M. Hoyer, G. Ephrem, W. A. Kay, *Int. J. Cardiol. Congenital Heart Dis.* **2021**, 6, 100287.
- [15] A. Rali, T. Buechler, B. Van-Gotten, E. Burgen, J. Chen, Z. Shah, N. Haglund, A. Sauer, *J. Am. Coll. Cardiol.* **2019**, 73, 819.
- [16] M. A. Chizner, *Curr. Probl. Cardiol.* **2008**, 33, 326.
- [17] O. T. Inan, P.-F. Migeotte, K.-S. Park, M. Etemadi, K. Tavakolian, R. Casanella, J. Zanetti, J. Tank, I. Funtova, G. K. Prisk, M. D. Rienzo, *IEEE J. Biomed. Health Inf.* **2014**, 19, 1414.
- [18] M. Etemadi, O. T. Inan, J. A. Heller, S. Hersek, L. Klein, S. Roy, *IEEE Trans. Biomed. Circuits Syst.* **2015**, 10, 280.
- [19] S. Preejith, R. Dhinesh, J. Joseph, M. Sivaprakasam, in *2016 38th Annual Int. Conf. of the IEEE Engineering in Medicine and Biology Society (EMBC)*, IEEE, Piscataway, NJ **2016**, pp. 623–626.
- [20] B. Semiz, A. M. Carek, J. C. Johnson, S. Ahmad, J. A. Heller, F. G. Vicente, S. Caron, C. W. Hogue, M. Etemadi, O. T. Inan, *IEEE J. Biomed. Health Inf.* **2020**, 25, 1572.
- [21] Y.-S. Hsu, T.-Y. Chen, D. Wu, C.-M. Lin, J.-N. Juang, W.-T. Liu, *J. Clin. Sleep Med.* **2020**, 16, 1149.
- [22] J. Li, J. Zhang, Y. Jiang, C. Ren, R. Guo, Y. Ma, Y. Qin, in *2022 44th Annual Int. Conf. of the IEEE Engineering in Medicine and Biology Society (EMBC)*, IEEE, Piscataway, NJ **2022**, pp. 4312–4315.
- [23] Y. Zhong, Y. Pan, L. Zhang, K.-T. Cheng, in *2016 38th Annual Int. Conf. of the IEEE Engineering in Medicine and Biology Society (EMBC)*, IEEE, Piscataway, NJ **2016**, pp. 603–606.
- [24] S. Lee, B. Grundlehner, R. G. van der Westen, S. Polito, C. Van Hoof, in *2019 41st Annual Int. Conf. of the IEEE Engineering in Medicine and Biology Society (EMBC)*, IEEE, Piscataway, NJ **2019**, pp. 1290–1293.
- [25] N. Verma, I. Haji-Abolhassani, S. Ganesh, J. Vera-Aguilera, J. Paludo, R. Heitz, S. N. Markovic, K. Kulig, A. Ghoreysy, *IEEE J. Transl. Eng. Health Med.* **2021**, 9, 2700407.
- [26] M. Di Rienzo, E. Vaini, P. Castiglioni, G. Merati, P. Meriggi, G. Parati, A. Faini, F. Rizzo, *Auton. Neurosci.* **2013**, 178, 50.
- [27] M. Di Rienzo, E. Vaini, P. Castiglioni, P. Lombardi, G. Parati, C. Lombardi, P. Meriggi, F. Rizzo, in *2014 36th Annual Int. Conf. of the IEEE Engineering in Medicine and Biology Society*, IEEE, Piscataway, NJ **2014**, pp. 6089–6091.
- [28] M. J. Tadi, T. Koivisto, M. Pänkäälä, A. Paasio, T. Knuutila, M. Teräs, P. Hänninen, in *Sixth Int. Conf. on Graphic and Image Processing (ICGIP 2014)*, vol. 9443, SPIE, Bellingham, WA **2015**, pp. 571–577.
- [29] T. Ha, J. Tran, S. Liu, H. Jang, H. Jeong, R. Mitbender, H. Huh, Y. Qiu, J. Duong, R. L. Wang, P. Wang, A. Tandon, J. Sirohi, N. Lu, *Adv. Sci.* **2019**, 6, 1900290.
- [30] M. Gonzalez, F. Axisa, M. V. Bulcke, D. Brosteaux, B. Vandeveld, J. Vanfleteren, *Microelectron. Reliab.* **2008**, 48, 825.
- [31] Y.-Y. Hsu, M. Gonzalez, F. Bossuyt, F. Axisa, J. Vanfleteren, I. De Wolf, *Thin Solid Films* **2011**, 519, 2225.
- [32] J. C. Edwards, J. B. Vander Veer, *Am. Heart J.* **1938**, 16, 431.
- [33] N. Ben-Dov, D. Gladstone, A. Micieli, E. Crystal, D. Newman, *J. Electrocardiol.* **2019**, 55, 54.
- [34] I. H. Hansen, K. Hoppe, A. Gjerde, J. K. Kanter, H. B. Sørensen, in *2015 37th Annual Int. Conf. of the IEEE Engineering in Medicine and Biology Society (EMBC)*, IEEE, Piscataway, NJ **2015**, pp. 330–333.
- [35] M. Chi, J. Zhao, Y. Dong, X. Wang, *Materials* **2019**, 12, 971.
- [36] H. Jang, K. Sel, E. Kim, S. Kim, X. Yang, S. Kang, K.-H. Ha, R. Wang, Y. Rao, R. Jafari, N. Lu, *Nat. Commun.* **2022**, 13, 6604.
- [37] A. Gruetzmänn, S. Hansen, J. Müller, *Physiol. Meas.* **2007**, 28, 1375.
- [38] R. S. Crow, P. Hannan, D. Jacobs, L. Hedquist, D. M. Salerno, *Am. J. Noninvasive Cardiol.* **1994**, 8, 39.
- [39] K. Sørensen, S. E. Schmidt, A. S. Jensen, P. Søgaard, J. J. Struijk, *Sci. Rep.* **2018**, 8, 15455.
- [40] M. Nikbakht, D. J. Lin, A. H. Gazi, O. T. Inan, *IEEE Sensors*, **2022**, doi: 10.1109/SENSORSS2175.2022.9967101.
- [41] M. Nikbakht, A. H. Gazi, J. Zia, S. An, D. J. Lin, O. T. Inan, R. Kamaleswaran, unpublished.
- [42] D. J. Lin, J. P. Kimball, J. Zia, V. G. Ganti, O. T. Inan, *IEEE Trans. Biomed. Eng.* **2021**, 69, 176.
- [43] M. M. H. Shandhi, B. Semiz, S. Hersek, N. Goller, F. Ayazi, O. T. Inan, *IEEE J. Biomed. Health Inf.* **2019**, 23, 2365.
- [44] J. Zia, J. Kimball, S. Hersek, O. T. Inan, *IEEE J. Biomed. Health Inf.* **2020**, 24, 1887.
- [45] J. Zia, J. Kimball, S. Hersek, M. M. H. Shandhi, B. Semiz, O. T. Inan, *IEEE J. Biomed. Health Inf.* **2019**, 24, 1080.
- [46] A. H. Gazi, S. Sundararaj, A. B. Harrison, N. Z. Gurel, M. T. Wittbrodt, M. Alkhalaf, M. Soudan, O. Levantsevych, A. Haffar, A. J. Shah, V. Vaccarino, J. D. Bremmer, O. T. Inan, in *43rd Annual Int. Conf. of the IEEE Engineering in Medicine and Biology Society (EMBC)*, IEEE, Piscataway, NJ **2021**, pp. 1444–1447.
- [47] H. Boudoulas, W. Barrington, S. M. Olson, T. M. Bashore, C. F. Wooley, *Am. Heart J.* **1985**, 110, 623.
- [48] R. A. Nelesen, J. E. Dimsdale, P. J. Mills, J. L. Clausen, M. G. Ziegler, S. Ancoli-Israel, *Sleep* **1996**, 19, 139.
- [49] G. S. Chan, P. M. Middleton, B. G. Celler, L. Wang, N. H. Lovell, *Physiol. Meas.* **2007**, 28, 439.
- [50] P. Dehkordi, F. Khosrow-Khavar, M. Di Rienzo, O. T. Inan, S. E. Schmidt, A. P. Blaber, K. Sørensen, J. J. Struijk, V. Zakeri, P. Lombardi, M. M. H. Shandhi, M. Borairi, J. M. Zanetti, K. Tavakolian, *Front. Physiol.* **2019**, 10, 1057.
- [51] M. Klum, M. Urban, T. Tigges, A.-G. Pielmus, A. Feldheiser, T. Schmitt, R. Orglmeister, *Sensors* **2020**, 20, 2033.
- [52] Y.-F. Yang, Y.-S. Chou, J.-Y. Wang, in *Proc. of Int. Conf. on Biomedical and Health Informatics*, Springer, Berlin **2019**, pp. 363–370.
- [53] S.-H. Liu, J.-J. Wang, C.-H. Su, D.-C. Cheng, *Sensors* **2018**, 18, 3036.
- [54] S. Yang, Y.-C. Chen, L. Nicolini, P. Pasupathy, J. Sacks, B. Su, R. Yang, D. Sanchez, Y.-F. Chang, P. Wang, D. Schnyer, D. Neikirk, N. Lu, *Adv. Mater.* **2015**, 27, 6423.

Supporting Information

for *Adv. Electron. Mater.*, DOI: 10.1002/aelm.202201284

A Chest-Conformable, Wireless Electro-Mechanical E-Tattoo for Measuring Multiple Cardiac Time Intervals

*Sarnab Bhattacharya, Mohammad Nikbakht, Alec Alden, Philip Tan, Jieting Wang, Taha A. Alhalimi, Sangjun Kim, Pulin Wang, Hirofumi Tanaka, Animesh Tandon, Edward F. Coyle, Omer T. Inan, and Nanshu Lu**

Supporting Information

A Chest-Conformable, Wireless Electro-Mechanical E-Tattoo for Measuring Multiple Cardiac Time Intervals

Sarnab Bhattacharya, Mohammad Nikbakht, Alec Alden, Philip Tan, Jieting Wang, Taha A Alhalimi, Sangjun Kim, Pulin Wang, Hirofumi Tanaka, Animesh Tandon, Edward F Coyle, Omer T Inan, Nanshu Lu*

S1 Supporting Figures

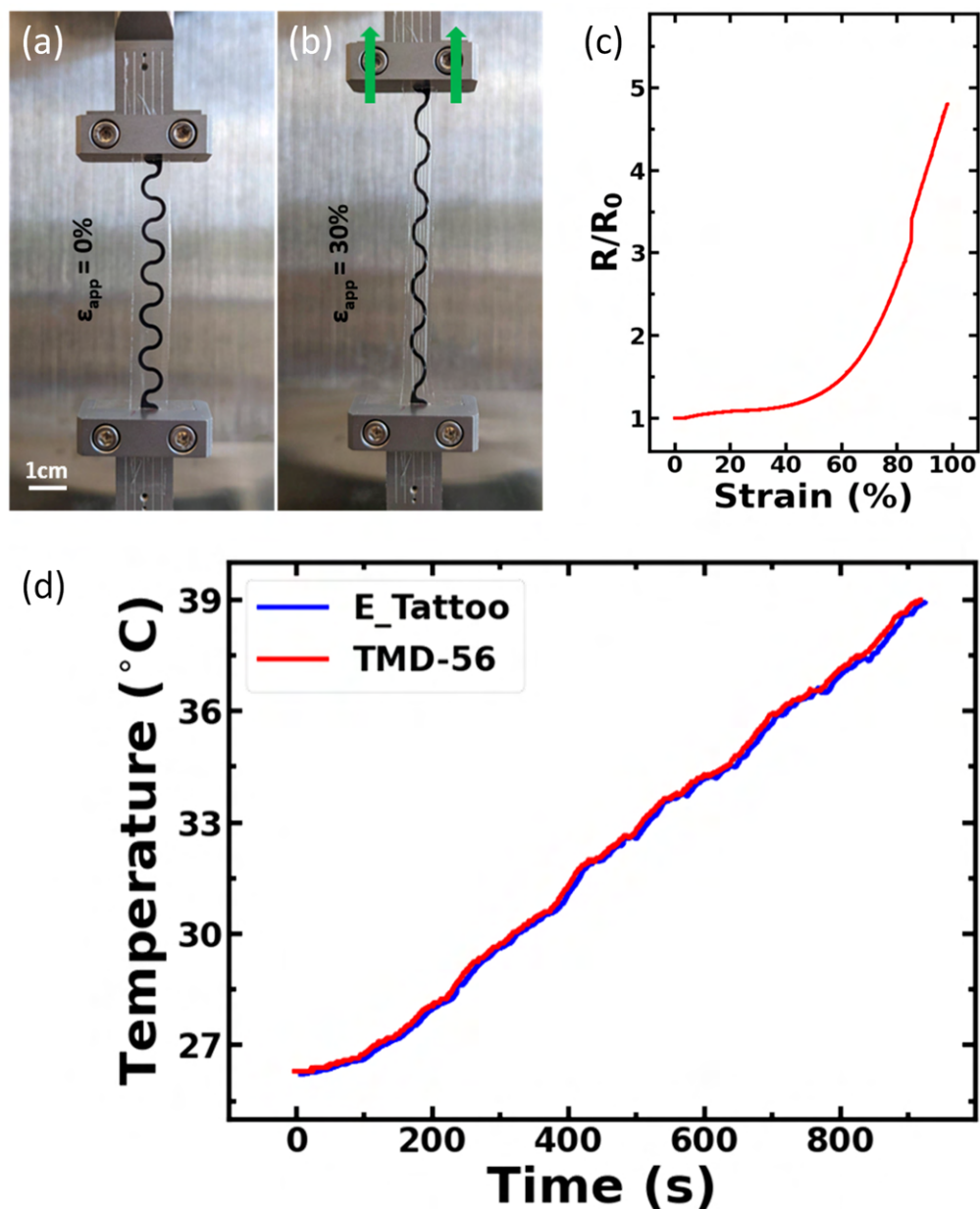


Figure S1: **Resistance change of electrode under strain.** a) Relaxed electrode and b) stretched to 30% strain. c) Resistance change under strain curve showing insignificant resistance change till 40% strain. d) E-tattoo temperature sensor validated against commercial thermistor over a range of temperatures (25-40°C).

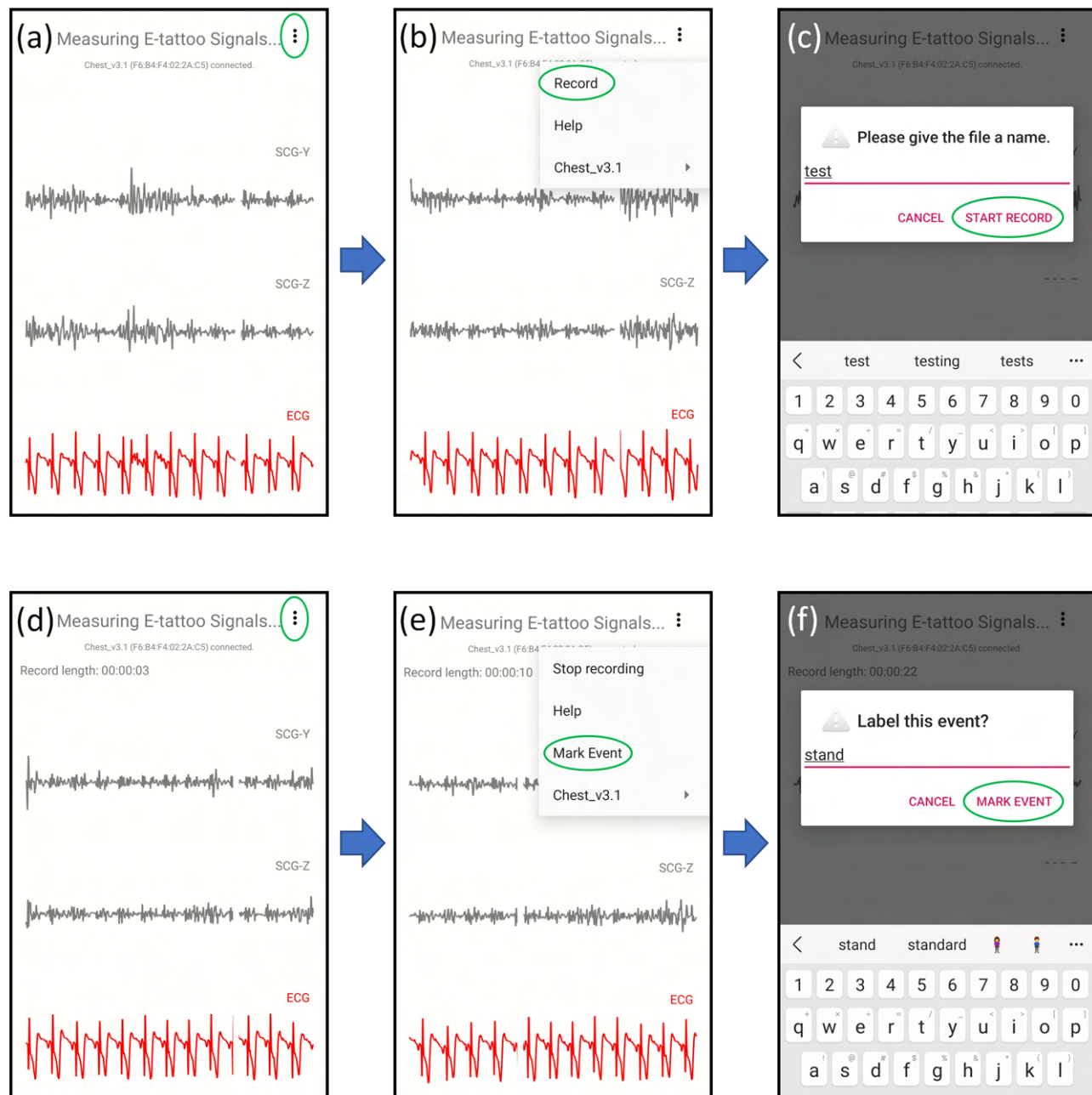
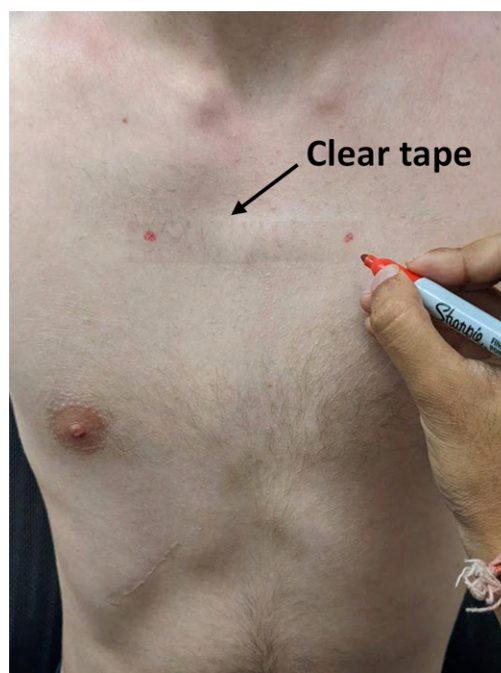


Figure S2: **Android application user guide.** a) Press upper 3-dot icon to open options menu, b) press *Record* to start a recording, c) type in an appropriate name for the recording and press *START RECORD*. d) While the application is recording data press on the 3-dot icon to open options again, e) press *Mark Event* option to annotate a user-defined event, f) type in an appropriate name and press *MARK EVENT*.



Subject	Compressed Strain	Stretched Strain
P1	11.0%	12.6%
P2	27.7%	13.8%
P3	25.5%	19.5%
P4	32.0%	14.0%
P5	21.3%	15.8%

Figure S3: **Human chest stretchability.** Locations of the electrodes were marked on the relaxed chest of the subjects. The subjects were then asked to stretch and compress their chest as much as possible without being uncomfortable. A clear tape was laminated during both stretching and compression, and the distance between the original marks was recorded. The change in length between the marks was used to calculate the compressive and tensile strains. The table on the right summarized the data obtained from the 5 participants. Stretching beyond 20% was not observed.

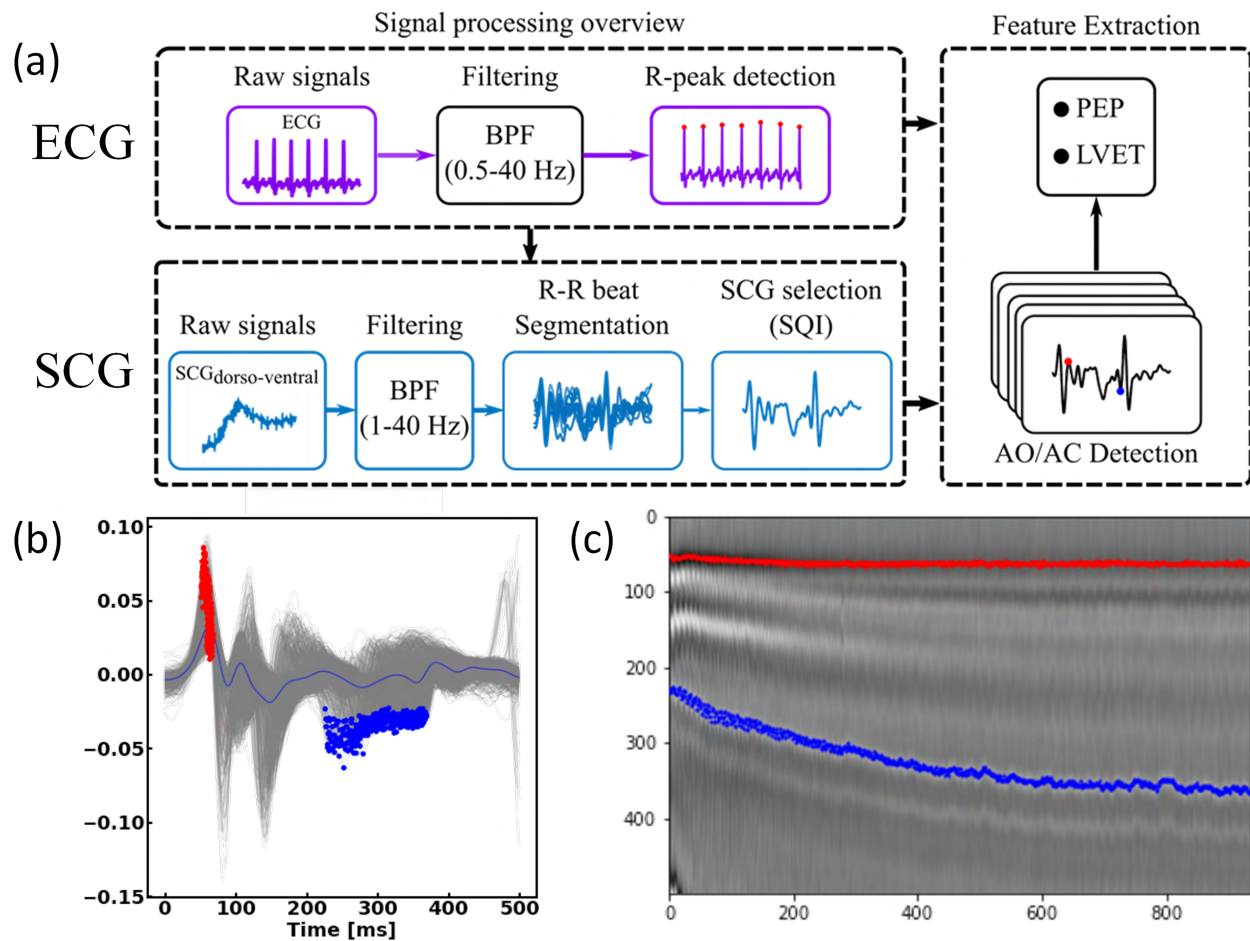


Figure S4: **Software processing pipeline.** a) Overview of the ECG and SCG data processing pipeline. The SCG signals are heart-beat separated using the ECG R-peaks and after rejecting the noisy beats, PEP and LVET features are extracted from the SCG beats. b) AO (marked with red) and AC (marked with blue) features on each SCG segment stacked over each other. c) Tracing of the change of AO and AC features during recovery. PEP: pre-ejection period; LVET: left ventricular ejection time; AO: aortic valve opening; AC: aortic valve closing.

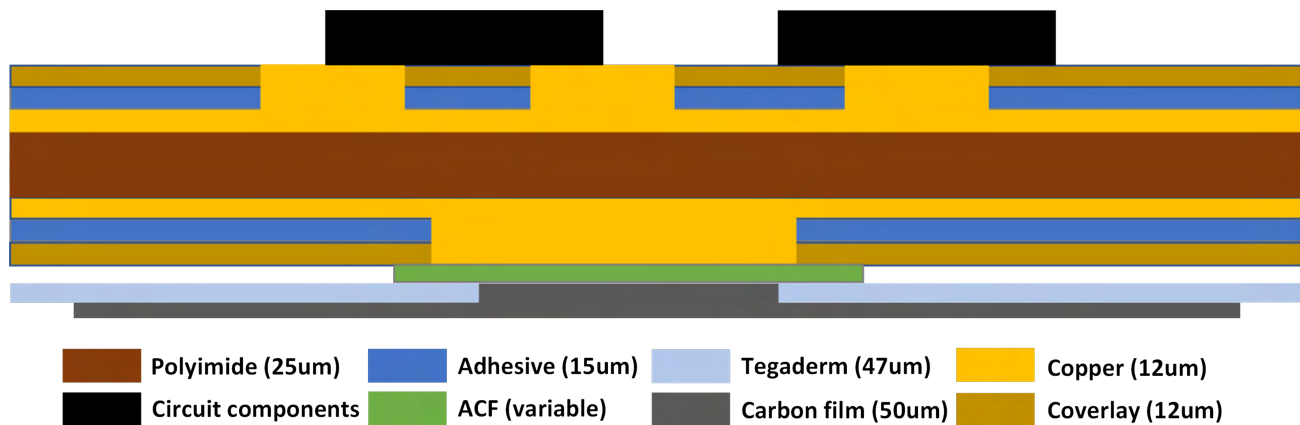


Figure S5: **Illustration of the cross-section of the e-tattoo.** Layers of the flexible printed circuit (FPC) and electrode are shown with thickness given in micrometer (um).

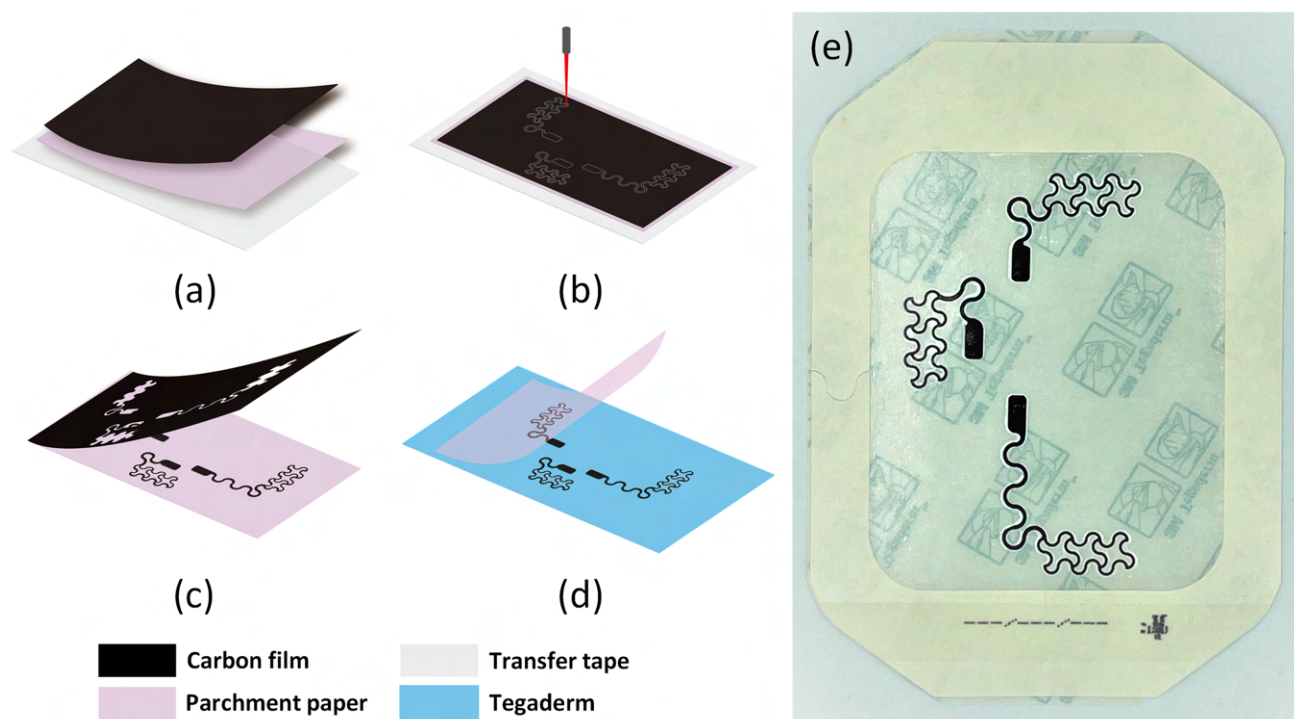


Figure S6: **Graphite film dry electrode manufacturing process.** Schematic illustration of the cut and transfer method used to make the carbon film dry electrode comprising a) laminating carbon film on parchment paper and transfer tape, b) laser cutting serpentine electrode pattern, c) removing excess carbon film, and d) transferring to Tegaderm. e) Ready-to-use electrode transferred onto a Tegaderm patch.

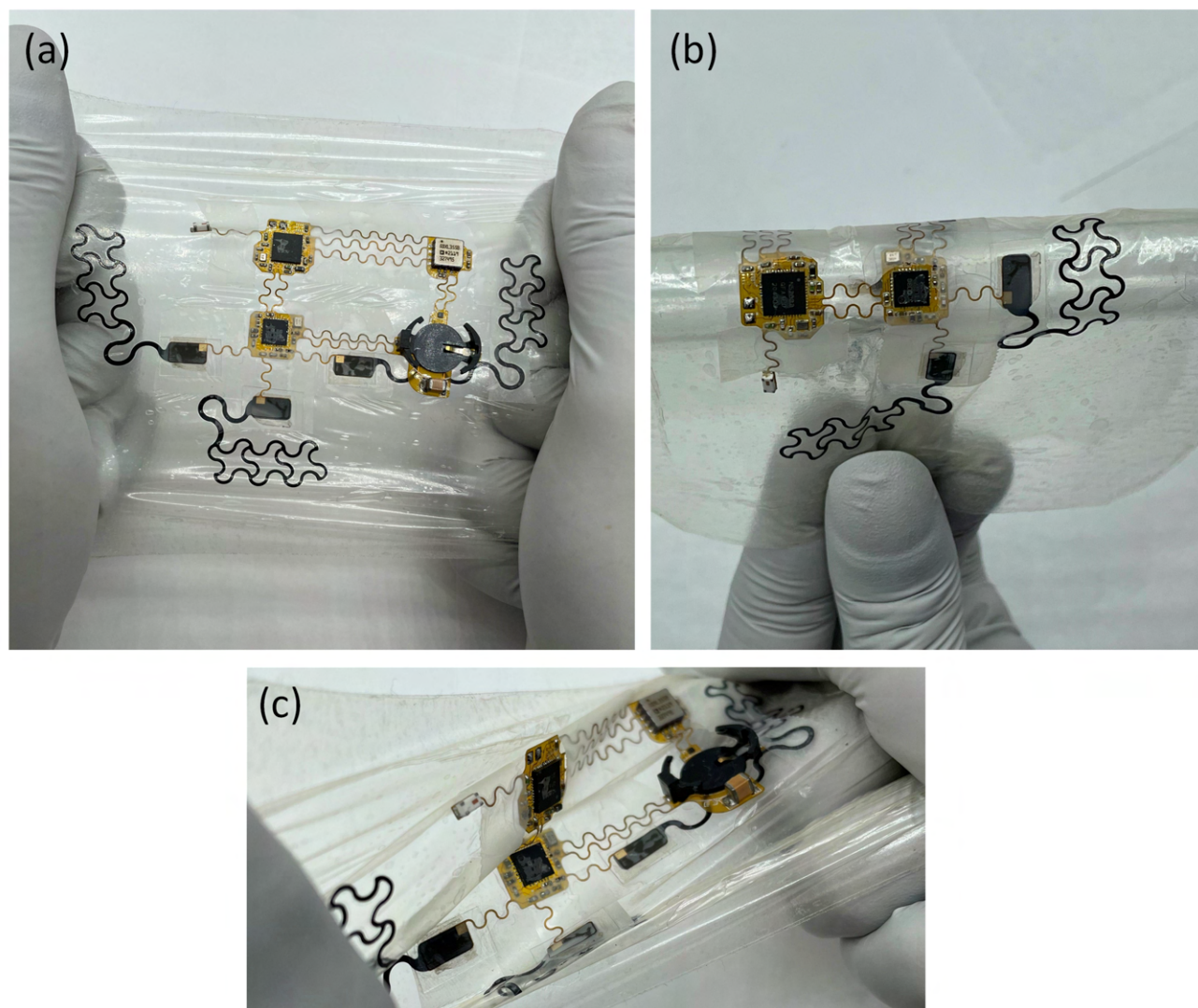


Figure S7: **Mechanical stress testing of e-tattoo.** a) Stretching, b) wrapping around a 16mm diameter glass rod, and c) twisting to illustrate the robustness and conformability of the e-tattoo.

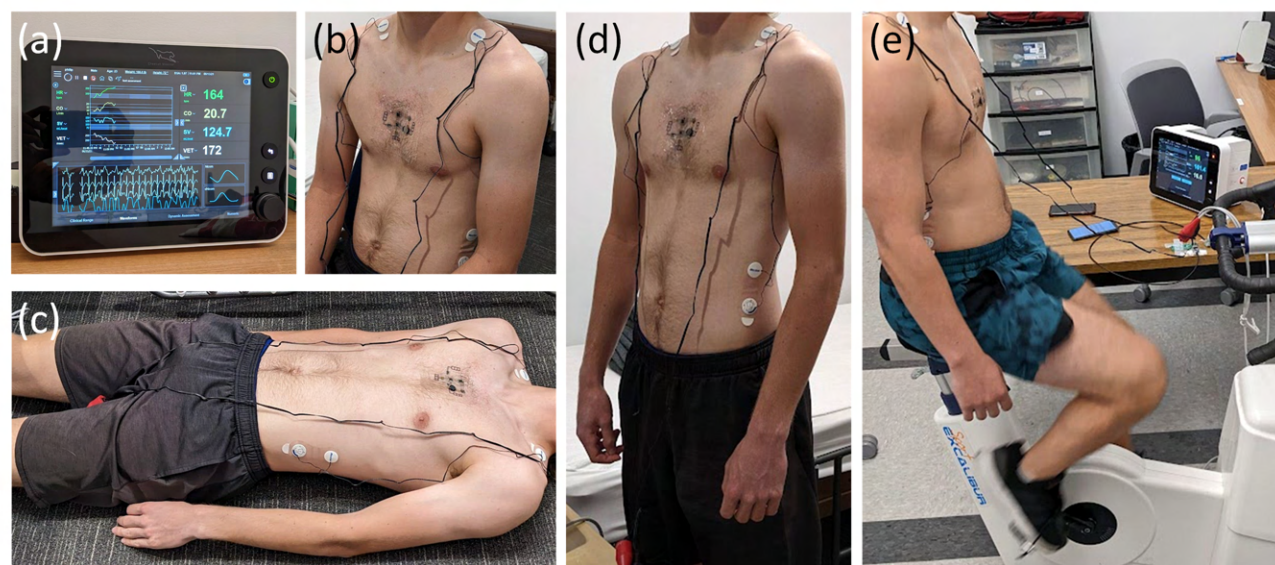


Figure S8: **Human subject testing.** a) Starling fluid management monitoring system from Baxter. It is an impedance cardiogram-based non-invasive cardiac output monitor (NICOM). NICOM and e-tattoo attached to a human subject for b) sitting upright, c) lying supine, and d) standing postures. e) NICOM and e-tattoo applied during cycling.

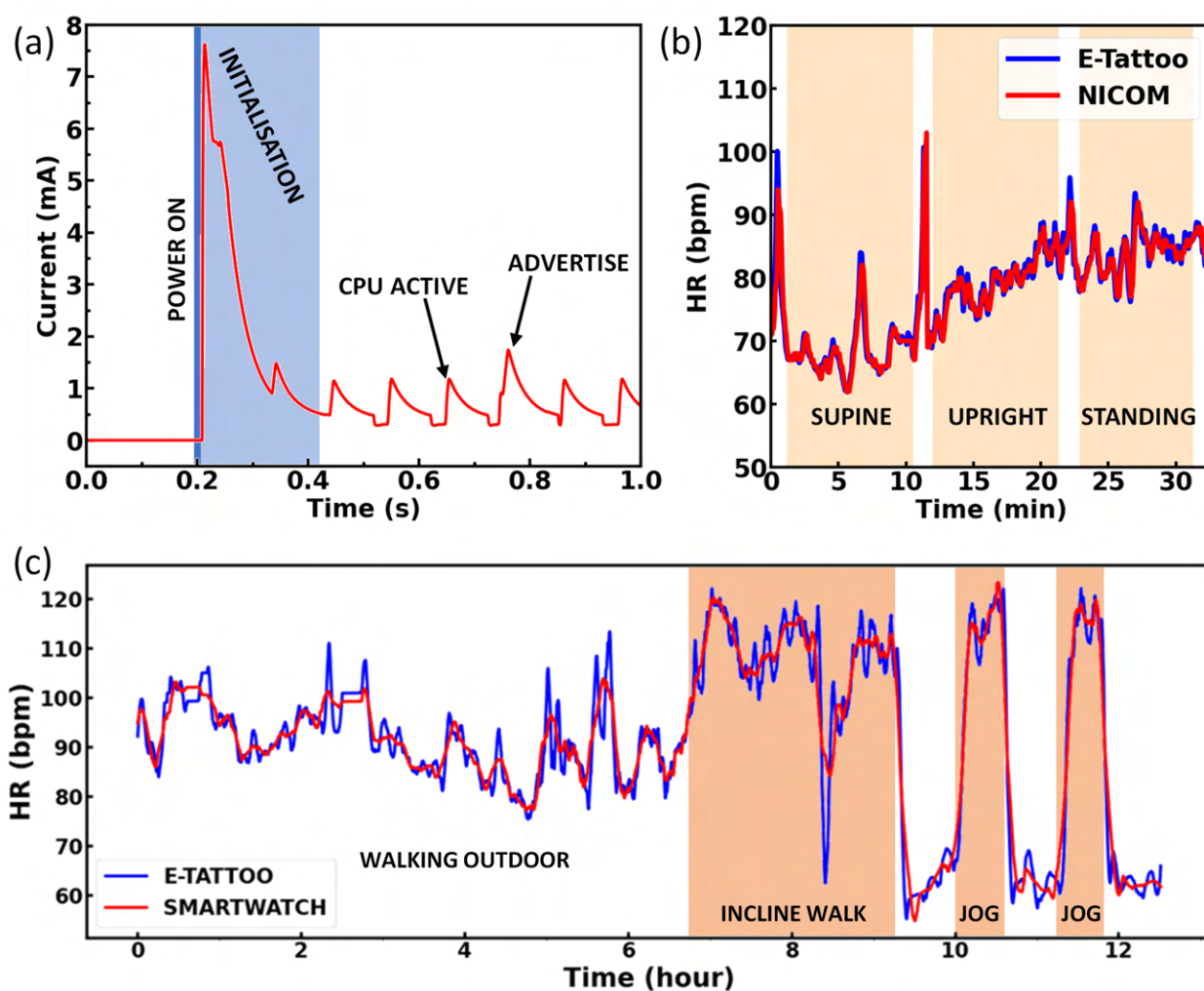


Figure S9: **Extra device characterisation.** a) Startup current draw profile. b) Time series heart rate (HR) data from the e-tattoo and the non-invasive cardiac output monitoring device during the static posture experiment illustrating the capability of the e-tattoo to detect short spikes in HR. c) Long-term study comparing HR from e-tattoo and commercial smartwatch (Samsung Galaxy S3).